CH_3 Internal Rotation in the S_0 and S_1 States of 9-Methylanthracene

Masaaki Baba,*,† Koichi Mori,† Motohisa Saito,† Yasuyuki Kowaka,† Yuki Noma,† Shunji Kasahara,‡ Takaya Yamanaka,§ Katsuhiko Okuyama,|| Takayoshi Ishimoto,⊥,# and Umpei Nagashima⊥,#

Department of Chemistry, Graduate School of Science, Kyoto University, Kyoto 606-8502, Japan, Molecular Photoscience Research Center, Kobe University, Nada-ku, Kobe 657-8501, Japan, Instrument Center, Institute for Molecular Science, Okazaki 444-8585, Japan, Department of Chemical Engineering and Materials, College of Engineering, Nihon University, Koriyama 963-8642, Japan, Research Institute for Computational Sciences, National Institute of Advanced Industrial Science and Technology, Umezono 1-1-1, Tsukuba, Ibaraki 305-8568, Japan, Core Research for Evolutional Science and Technology, Japan Science and Technology Agency, 4-1-8 Honcho, Kawaguchi 332-0012, Japan

Received: September 26, 2008; Revised Manuscript Received: January 6, 2009

Fluorescence excitation spectra and dispersed fluorescence spectra of jet-cooled 9-methylanthracene-h_{12} and -d_{12} (9MA-h_{12} and 9MA-d_{12}) have been observed, and the energy levels of methyl internal rotation (CH_3 torsion) in the S_0 and S_1 states have been analyzed. The molecular symmetry of 9MA is the same as that of toluene (G_{12}). Because of two-fold symmetry in the π system, the potential curve has six-fold barriers to CH_3 rotation. In toluene, the barrier height to CH_3 rotation V_6 is very small, nearly free rotation. As for 9MA-h_{12}, we could fit the level energies by potential curves with the barrier heights of $V_6(S_0) = 118$ cm^{-1} and $V_6(S_1) = 33$ cm^{-1}. These barrier heights are remarkably larger than those of toluene and are attributed to hyperconjugation between the π orbitals and methyl group. The dispersed fluorescence spectrum showed broad emission for the excitation of $0_0^0 + 386$ cm^{-1} band, indicating that intramolecular vibrational redistribution efficiently occurs, even in the vibronic level of low excess energy of the isolated 9MA molecule.

1. Introduction

Methyl derivatives of polycyclic aromatic hydrocarbons show characteristic excited-state dynamics that depend on the barrier height to CH_3 internal rotation (torsion) and level energies.[1−9] There are two factors for the origin of the barrier, that is, the steric hindrance of hydrogen atoms and the interaction between the CH_3 sp^3 and π orbitals, which is called hyperconjugation.[10,11] The latter has been shown to be dominant in acetaldehyde, which is one of the prototypical methyl carbonyl compounds.[12,13]

In toluene, which is one of the prototypical methyl aromatic hydrocarbons, the barrier height is very small and the CH_3 rotation is considered to be almost free. The two-fold axis of the benzene moiety coincides with the three-fold axis of the CH_3 group. Therefore, it is expected that the barrier height to rotation is smaller than that of other methyl derivatives because the potential curve has only the six-fold component. It is of great interest to investigate 9MA, which has the same symmetry as toluene, and there have been several spectroscopic studies of 9MA in a supersonic jet.[14−17] However, the assignments of vibronic bands observed in the fluorescence excitation spectrum of the $S_1 \leftarrow S_0$ transition are not reliable, and the energies of CH_3 torsional levels have not yet been determined for certain.

We carefully observed the spectra again for 9MA-h_{12} and 9MA-d_{12} and made correct assignments by the results of double-resonance (hole-burning) experiments and dispersed fluorescence spectra for the single-vibronic-level excitation. In this article, we present these experimental results and discuss the level structure and excited-state dynamics in the isolated 9MA molecule. We also present the results of ab initio theoretical calculations and discuss the origin of the barrier to CH_3 internal rotation.

2. Experimental Section

9MA-h_{12} (Wako Chemical) was recrystallized from ethanol and heated to 150 °C in a stainless steel container. 9MA-d_{12} (CDN Isotopes) was used without further purification. The vapor was mixed with Ar gas, and the mixed gas was expanded from a pulsed nozzle (automobile fuel injector) into a high vacuum chamber to generate a supersonic jet. We used a pulsed dye laser (Lambda Physik, LPD 3000, Exalite 367 dye, $\Delta E = 0.1$ cm^{-1}) pumped by an excimer laser (Lambda Physik, LPX 105i, 308 nm, 100 mJ) as a light source. Fluorescence was focused by a lens to a photomultiplier (Hamamatsu R928), and the output was processed by a box-car integrator (Stanford Research, SR 200). We observed the fluorescence excitation spectrum by recording the change in fluorescence intensity with the wavelength of laser light by tuning the wavelength to a prominent vibronic band (probe laser). The dispersed fluorescence spectrum was observed using a monochromator with a focal length of 250 mm (Nikon, P250). Another laser light (pump laser) was irradiated 500 ns before the probe laser, and we observed the double-resonance fluorescence-dip (hole-burning) spectrum by recording the change in fluorescence intensity with the wavelength of the pump laser. We used a dye laser (Lambda Physik, Scanmate OPPO, $\Delta E = 0.1$ cm^{-1}) pumped by a YAG laser (Spectra Physics, GCR-200-10, 355 nm, 50 mJ) as a light source of the pump laser.

* To whom correspondence should be addressed. E-mail: baba@kuchem.kyoto-u.ac.jp.
† Kyoto University.
‡ Kobe University.
§ Institute for Molecular Science.
|| Nihon University.
⊥ National Institute of Advanced Industrial Science and Technology.
Japan Science and Technology Agency.

10.1021/jp808550r CCC: $40.75
Published on Web 02/20/2009

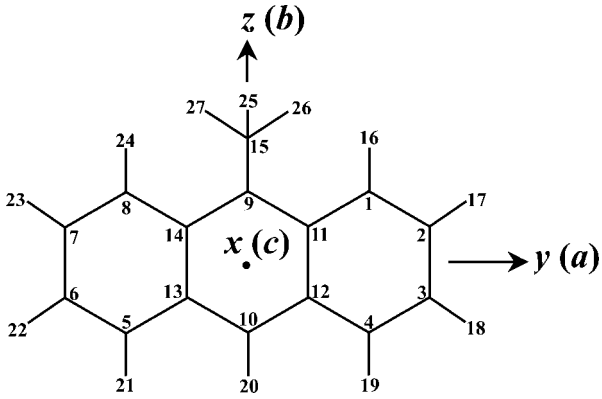

Figure 1. Coordinate and rotational axes of the 9-methylanthracene (9MA) molecule.

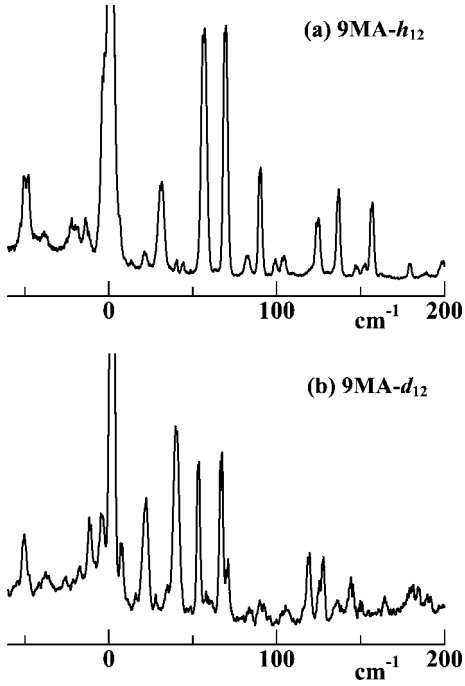

Figure 2. Fluorescence excitation spectra of the $S_1 \leftarrow S_0$ transitions of (a) 9MA-h_{12} and (b) 9MA-d_{12} in supersonic jets.

3. Results and Discussion

The coordinate and rotational axes of 9MA are shown in Figure 1. We take the z axis parallel to the short axis of the anthracene plane, which coincides with the CH_3 rotation axis. The y axis is parallel to the long axis, and the x axis is out-of-plane. The 9MA molecule is an asymmetric top. The principal axis (a) is the long axis (y). The b and c axes are parallel to z and x, respectively. The CH_3 rotation is six-fold symmetric, and two conformations should be considered. One is "staggered," in which one of the three H atoms is in the xz plane. Another is "eclipsed," in which an H atom is in the yz plane.

In Figure 2 are shown the fluorescence excitation spectra in the low excess energy region of the $S_1 \leftarrow S_0$ transitions of 9MA-h_{12} and 9MA-d_{12} in supersonic jets. The 0_0^0 band of 9MA-h_{12} is observed at 26931 cm^{-1}, and relatively strong vibronic bands are seen at 57 and 69 cm^{-1}. To assign these bands, one must consider the changes of level energies with respect to barrier height to CH_3 rotation. The molecular symmetry group of 9MA is G_{12} with a three-fold axis of CH_3 group and a two-fold axis of anthracene moiety.[18−20] The potential curve has six-fold symmetry with respect to the CH_3 rotational angle, ϕ. The 1D Schrödinger equation is expressed as

$$\left\{-F\frac{\partial^2}{\partial\phi^2}+\frac{V_6}{2}(1-\cos 6\phi)\right\}\Psi = E_m\Psi \quad (1)$$

where F is the CH_3 rotational constant and is estimated to be 5.4 cm^{-1} by the theoretical calculation shown later. If the barrier height to CH_3 rotation $V_6 = 0$ (unhindered rigid rotor), then the eigenvalues are

$$E_m = m^2F, \quad m = 0, \pm1, \pm2, \ldots \quad (2)$$

and the eigenfunctions are expressed by

$$\Psi_m(\phi) = \frac{1}{\sqrt{2\pi}}\,e^{\pm im\phi} \quad (3)$$

$\Psi_0(\phi)$ is constant. In the case of a hindered rigid rotor ($V_6 \neq 0$), the eigenvalues and eigenfunctions are obtained by diagonalization of the energy matrix. The nonvanishing matrix elements are[2]

$$<m|H|m> = Fm^2 + \frac{V_6}{2} \quad (4)$$

$$<m|H|m\pm6> = -\frac{V_6}{4} \quad (5)$$

The eigenfunctions are expressed as the linear combinations of $\Psi_m(\phi)$. The energy levels of CH_3 torsion for $F = 5.4$ cm^{-1} are

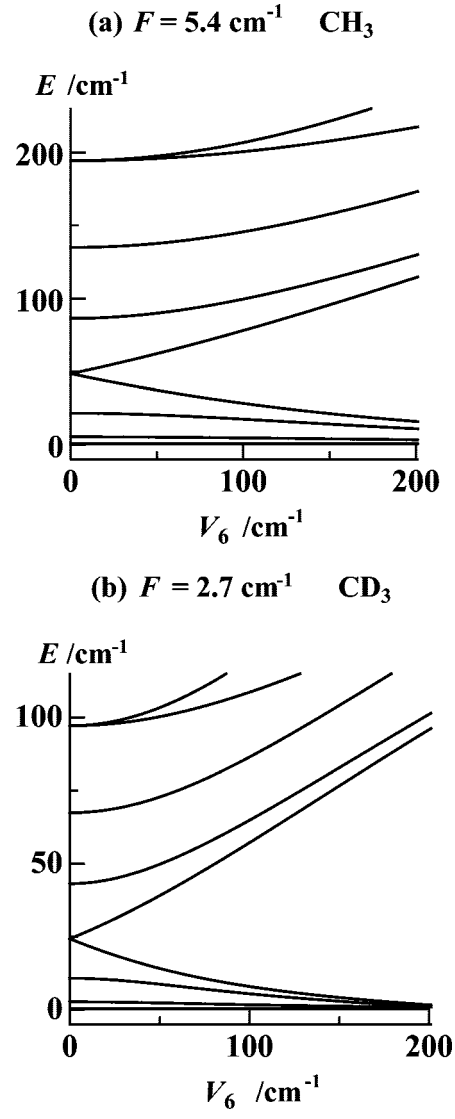

Figure 3. (a) CH_3 ($F = 5.4$ cm^{-1}) and (b) CD_3 ($F = 2.7$ cm^{-1}) torsional levels with respect to V_6.

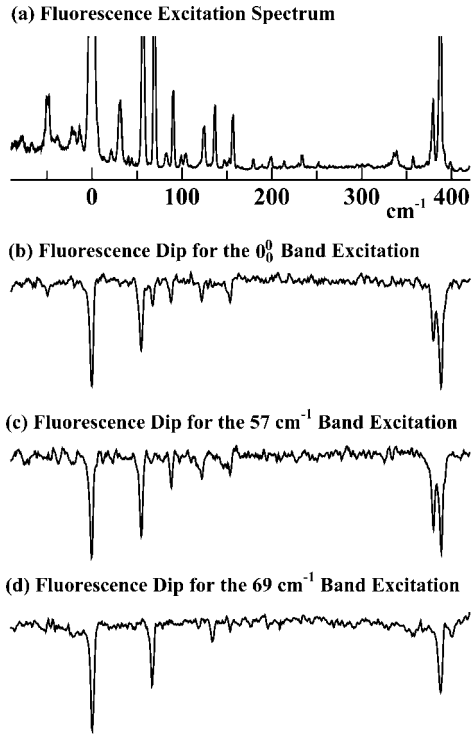

Figure 4. Optical−optical doule-resonance fluorescence-dip spectra (hole-burning spectra) of the $S_1 \leftarrow S_0$ transition of 9MA-h_{12} in a supersonic jet.

TABLE 1: Vibrational Energies and Assignments of the Observed Vibronic Bands in the Fluorescence Excitation Spectra of the $S_1 \leftarrow S_0$ Transitions of 9MA-h_{12} and 9MA-d_{12}

9MA-h_{12}		9MA-d_{12}	
vibrational energy	assignments	vibrational energy	assignments
−51		−50	
−24		−12	
−15		−5	
0	$0a_1' \leftarrow 0a_1'$ (26 931 cm^{-1})	0	$0a_1' \leftarrow 0a_1'$ (27 005 cm^{-1})
1	$1e'' \leftarrow 1e''$	1	$1e'' \leftarrow 1e''$
31		22	
57	$3a_1'' \leftarrow 0a_1'$	40	$3a_1'' \leftarrow 0a_1'$
69	$4e' \leftarrow 1e''$	53	$4e' \leftarrow 1e''$
82			
90	$3a_1'' \leftarrow 0a_1' + 33$	67	$3a_1'' \leftarrow 0a_1' + 27$
98			
103			
123	$3a_1'' \leftarrow 0a_1' + 33 \times 2$	91	$3a_1'' \leftarrow 0a_1' + 27 \times 2$
136		118	$3a_1'' \leftarrow 0a_1' + 27 \times 3$
156	$3a_1'' \leftarrow 0a_1' + 33 \times 3$	128	
178		145	
198		170	
213		182	
231		185	
335		217	
356		322	
377		362	
386		372	

shown in Figure 3a. The G_{12} molecular symmetry group is isomorphous with the D_{3h} point group, and the energy levels are represented as $0a_1'$, $1e''$, $2e'$, $3a_2''$, $3a_1''$, $4e'$, $5e''$, $6a_2'$, $6a_1'$, $7e''$, and so on.

The $3a_1'' \leftarrow 0a_1'$ and $4e' \leftarrow 1e''$ bands are strongly observed in toluene and phenylsilane.[1,2] The $0_0^0 + 57$ cm^{-1} and $0_0^0 + 69$ cm^{-1} bands of 9MA are analogically assigned to them, respectively. To confirm the assignments we observed the double-resonance fluorescence-dip spectrum (hole-burning spectrum) when we tuned the probe laser wavelength to a single vibronic band and scanned the wavelength of the pump laser (Figure 4). When we tuned the probe laser to the $0_0^0 + 57$ cm^{-1} band, we observed fluorescence dips at 0, 57, 90, 123, and 156 cm^{-1}. These bands are all assigned to the transitions between the levels of a symmetry because the $a \leftrightarrow e$ transition is forbidden. However, we observed fluorescence dips at 1, 69, and 136 cm^{-1} for the $0_0^0 + 69$ cm^{-1} band excitation. These bands are assigned to the $e \leftrightarrow e$ transitions.

By these observations, we could certainly assign several vibronic bands, and the results are listed in Table 1. The energies of CH_3 torsional levels were determined by transition energies of the observed vibronic bands. First, we changed the V_6 term and tried

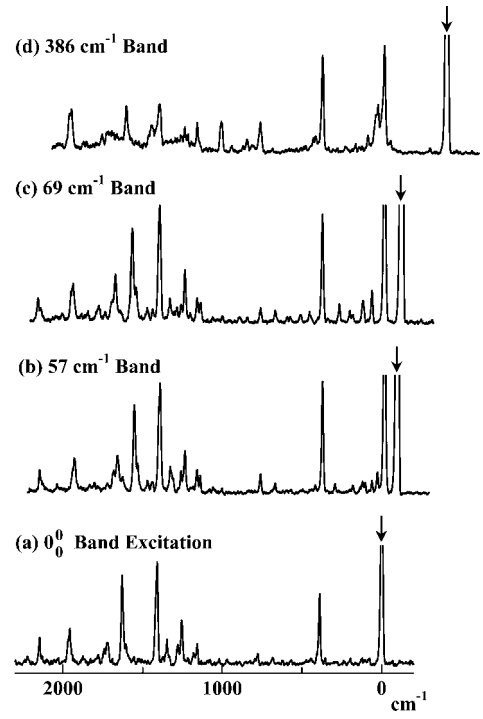

Figure 5. Dispersed fluorescence spectra for the single vibronic excitations of the $S_1 \leftarrow S_0$ transition of 9MA-h_{12} in a supersonic jet. The arrows indicate the positions of excitation laser light.

TABLE 2: Observed Energies of Methyl Torsional Levels of 9MA-h_{12} and 9MA-d_{12} and Calculated Ones Using the Best-Fit Potentials[a]

	9MA-h_{12}			9MA-d_{12}	
S_0	calcd	(obsd)		calcd	(obsd)
$0a_1'$	0	(0)	$0a_1'$	0	(0)
$1e''$	4.5		$1e''$	1.9	
$2e'$	16		$2e'$	6	
$3a_2''$	26		$3a_2''$	10	
$3a_1''$	84	(80)	$3a_1''$	52	(49)
$4e'$	104	(109)	$4e'$	60	(62)
$5e'$	150		$5e'$	82	
	$F = 5.4$ cm^{-1}	$V_6 = 118$ cm^{-1}		$F = 2.7$ cm^{-1}	$V_6 = 85$ cm^{-1}
	9MA-h_{12}			9MA-d_{12}	
S_1	calcd	(obsd)		calcd	(obsd)
$0a_1'$	0	(0)	$0a_1'$	0	(0)
$1e''$	5.3		$1e''$	2.3	
$2e'$	21		$2e'$	8	
$3a_2''$	41		$3a_2''$	14	
$3a_1''$	57	(57)	$3a_1''$	40	(40)
$4e'$	88	(74)	$4e'$	51	(51)
$5e'$	136		$5e'$	74	
	$F = 5.4$ cm^{-1}	$V_6 = 33$ cm^{-1}		$F = 2.7$ cm^{-1}	$V_6 = 54$ cm^{-1}

[a] All energies are the difference from the $0a_1'$ level.

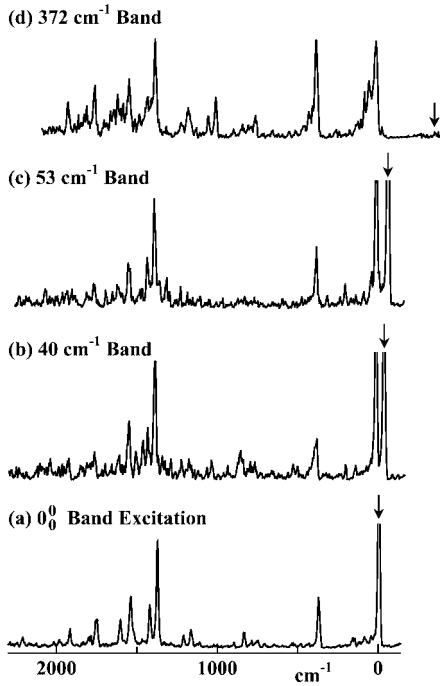

Figure 6. Dispersed fluorescence spectra for the single vibronic excitations of the $S_1 \leftarrow S_0$ transition of 9MA-d_{12} in a supersonic jet. The arrows indicate the positions of excitation laser light.

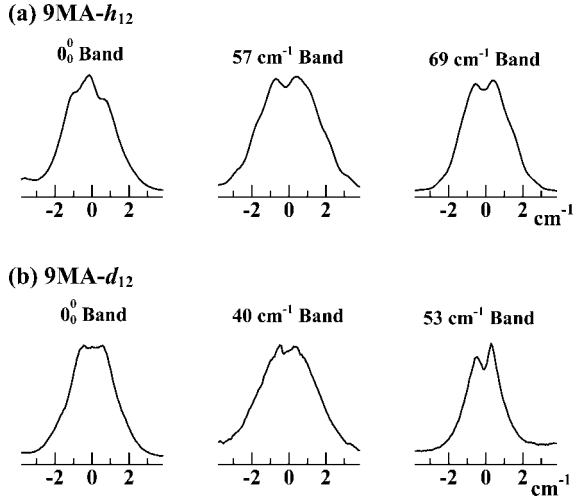

Figure 7. Rotational envelopes of (a) 0_0^0 ($0a_1' \leftarrow 0a_1' + 1e'' \leftarrow 1e''$), 57 cm^{-1} ($3a_1'' \leftarrow 0a_1'$), and 69 cm^{-1} ($4e' \leftarrow 1e''$) bands of 9MA-h_{12} and (b) 0_0^0 ($0a_1' \leftarrow 0a_1' + 1e'' \leftarrow 1e''$), 40 cm^{-1} ($3a_1'' \leftarrow 0a_1'$), and 53 cm^{-1} ($4e' \leftarrow 1e''$) bands of 9MA-d_{12}.

to fit the energies of the $3a_1''$ and $4e'$ levels using the 1D CH_3 rotation model fixing the F value to 5.4 cm^{-1}. The level energies in the S_0 state were determined by dispersed fluorescence spectra for excitations of the $3a_1''$ and $4e'$ levels in the S_1 state (Figure 5). We could obtain satisfactory fits with $V_6(S_0) = 118$ cm^{-1} and $V_6(S_1) = 33$ cm^{-1}, except for the $4e'$ level in the S_1 state. This level energy is evidently lower than that expected with this F value, and we did not include this level energy in the final fit. These results are tabulated in Table 2.

To check the validity of these assignments, we also analyzed the fluorescence excitation spectrum of 9MA-d_{12} (Figure 2b). The energy levels of CD_3 torsion for $F = 2.7$ cm^{-1} are shown in Figure 3b. The observed vibronic bands and assignments are listed in Table 1. The $0_0^0 + 40$ cm^{-1} and $0_0^0 + 53$ cm^{-1} bands are assigned to the $3a_1'' \leftarrow 0a_1'$ and $4e' \leftarrow 1e''$ transitions, respectively. The level energies in the S_0 state were determined

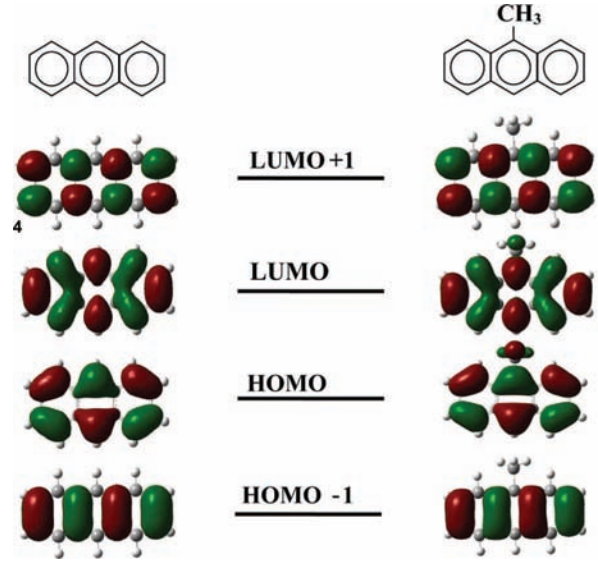

Figure 8. Calculated π molecular orbitals of anthracene and 9MA at the B3LYP/6-31G** level.

by the dispersed fluorescence spectra (Figure 6). By the same procedure as that for 9MA-h_{12}, we obtained $V_6(S_0) = 85$ cm^{-1} and $V_6(S_1) = 54$ cm^{-1} for 9MA-d_{12}. The results are also shown in Table 2. Although the V_6 values are slightly different between 9MA-h_{12} and 9MA-d_{12}, the assignments of vibrational bands are considered to be reasonable. In principle, the potential curve of CH_3 torsion is different from that of CD_3 because the 1s orbital of a D atom is slightly smaller than that of a H atom.[21] The V_6 value is appreciably changed by deuteration, particularly in the case of low barrier height.

We further observed rotational envelopes of the 0_0^0, $3a_1'' \leftarrow 0a_1'$, and $4e' \leftarrow 1e''$ bands of both 9MA-h_{12} and 9MA-d_{12}. The results are shown in Figure 7. The spectral feature of the 0_0^0 band of 9MA-h_{12} are strange. However, the envelope is easily explained by the overlap of two b-type bands with the splitting of 1 cm^{-1}. These are assigned to the $0a_1' \leftarrow 0a_1'$ and $1e'' \leftarrow 1e''$ transitions. The rotational envelope depends on the direction of the electronic transition moment. To understand the $S_1 \leftarrow S_0$ transition of 9MA, we performed ab initio theoretical calculations using the Gaussian 03 program package.[22] The calculated molecular orbitals of the anthracene and 9MA molecules are shown in Figure 8. The S_1 $^1B_{2u} \leftarrow S_0$ ^1A_g transition of anthracene is approximately expressed by the single configuration of HOMO $\rightarrow$ LUMO electronic excitation. This is a strong transition in which the transition moment is parallel to the in-plane short axis. This axis is the rotational b axis, and the selection rules for the b-type transition are $\Delta J = 0, \pm 1$; $\Delta K_a = \pm 1$; and $\Delta K_c = \pm 1$.[23] The rotational envelope shows two intensity maxima of P and R transitions without a sharp Q peak at the band center. The observed rotational envelope of the $0a_1' \leftarrow 0a_1'$ band of 9MA shows this b-type feature, and the transition moment is parallel to the short axis in the anthracene plane and also the CH_3 rotation axis.

The selection rules for the optical transitions between the CH_3 torsional levels depend on the symmetries of the levels.[18] The selection rules in G_{12} for the electronic transition in the three directions are as follows

z (b-type): $a_1' \leftrightarrow a_1', a_1'' \leftrightarrow a_1'', a_2' \leftrightarrow a_2', a_2'' \leftrightarrow a_2'', e' \leftrightarrow e', e'' \leftrightarrow e''$

y (a-type): $a_1' \leftrightarrow a_2'', a_2' \leftrightarrow a_2'', e' \leftrightarrow e''$

x (c-type): $a_1' \leftrightarrow a_1'', a_2' \leftrightarrow a_2'', e' \leftrightarrow e''$

Only the transition between the levels of identical symmetry possesses the transition moment in the z direction. Therefore,

TABLE 3: Calculated Coordinates (*x*, *y*, *z* in Å) and Mulliken Atomic Charge (AC) of Individual Atoms in the Staggered ($\phi = 0°$) and Eclipsed ($\phi = 30°$) Conformations Calculated by Gaussian 03 at the MP2/6-31G Level.**

	staggered $\phi = 0°$				eclipsed $\phi = 30°$			
atom	*x*	*y*	*z*	AC	*x*	*y*	*z*	AC
C1	−0.0293	2.4957	1.1488	−0.1394	0.0000	2.4916	1.1369	−0.1396
C2	0.0614	3.6683	0.4305	−0.1599	0.0000	3.6636	0.4159	−0.1598
C3	−0.0188	3.6540	−0.9875	−0.1608	0.0000	3.6439	−1.0026	−0.1620
C4	−0.0071	2.4547	−1.6548	−0.1267	0.0000	2.4429	−1.6687	−0.1246
C5	−0.0054	−2.4527	−1.6571	−0.1266	0.0000	−2.4644	−1.6447	−0.1264
C6	−0.0200	−3.6522	−0.9898	−0.1609	0.0000	−3.6632	−0.9773	−0.1612
C7	0.0606	−3.6671	0.4281	−0.1597	0.0000	−3.6756	0.4413	−0.1632
C8	0.0274	−2.4947	1.1467	0.1400	0.0000	−2.5027	1.1590	0.1324
C9	−0.0522	−0.0003	1.2081	0.0049	0.0000	0.0031	1.2109	0.0164
C10	−0.0290	0.0014	−1.6307	−0.1524	0.0000	−0.0144	−1.6317	−0.1557
C11	0.0101	1.2230	0.4986	−0.0312	0.0000	1.2198	0.4865	−0.0445
C12	−0.0435	1.2191	−0.9448	−0.0117	0.0000	1.2091	−0.9554	−0.0102
C13	−0.0429	−1.2175	−0.9467	−0.0114	0.0000	−1.2268	−0.9363	−0.0127
C14	0.0096	−1.2223	0.4963	−0.0310	0.0000	−1.2277	0.5108	−0.0498
C15	−0.0680	−0.0064	2.7163	−0.3485	0.0000	0.0690	2.7180	−0.3455
H16	0.0851	2.5471	2.2270	0.1524	0.0000	2.5406	2.2172	0.1559
H17	0.0933	4.6151	0.9555	0.1499	0.0000	4.6132	0.9371	0.1506
H18	0.0404	4.5859	−1.5384	0.1518	0.0000	4.5754	−1.5548	0.1524
H19	−0.0335	2.4270	−2.7387	0.1515	0.0000	2.4125	−2.7528	0.1533
H20	−0.0641	0.0023	−2.7162	0.1514	0.0000	−0.0241	−2.7178	0.1562
H21	−0.0308	−2.4249	−2.7410	0.1516	0.0000	−2.4354	−2.7289	0.1528
H22	0.0426	−4.5839	−1.5411	0.1518	0.0000	−4.5965	−1.5263	0.1524
H23	0.0914	4.6143	0.9527	0.1500	0.0000	−4.6224	0.9674	0.1503
H24	0.0802	−2.5453	2.2252	0.1527	0.0000	−2.5631	2.2378	0.1546
H25	0.9403	−0.0427	3.1349	0.1266	0.8797	0.6013	3.0827	0.1355
H26	−0.5608	0.8788	3.1100	0.1380	−0.8796	0.6014	3.0827	0.1355
H27	−0.6182	−0.8629	3.0988	0.1277	0.0000	−0.9120	3.1801	0.1217

the $0a' \leftarrow 0a'$ and $1e'' \leftarrow 1e''$ bands are expected to be strong because the $S_1 \leftarrow S_0$ transition moment is large and parallel to the *z* direction. The energy splitting between the $0a_1'$ and $1e''$ levels takes the largest value at $V_6 = 0$; still, it is very small (5.4 cm^{-1}). Therefore, the two bands are overlapped at an almost identical transition energy. The difference in 9MA is about 1 cm^{-1}. Although calculations of rotational energies are complicated and it is not easy to simulate the observed rotational envelope, the energy difference between the $0a_1' \leftarrow 0a_1'$ and $1e'' \leftarrow 1e''$ transitions can be estimated to be 1.0 ± 0.2 cm^{-1}. It indicates that $V_6(S_0)$ is larger than $V_6(S_1)$ by more than 50 cm^{-1}.

The $3a_1'' \leftarrow 0a_1'$ band is expected to be the *c*-type transition. However, the observed rotational envelope clearly shows the *b*-type feature. The electronic transition moment in the *c* direction (out-of-plane) arises from the $\sigma\pi^*$ state and is supposed to be very small. It is considered that the intensity is brought by the second-order borrowing from the strong *b*-type transition. The $4e' \leftarrow 1e''$ band is expected to be the *a*- or *c*-type transition. However, the observed rotational envelope also shows the *b*-type feature. It is explained in the same manner as the $3a_1'' \leftarrow 0a_1'$ band. Further studies are necessary to understand the relatively strong intensities of these two bands. Nakagaki et al.[17] have already reported assignments of the CH_3 torsion levels of 9MA-h_{12}. They fitted the level energies by a 2D potential including an out-of plane vibration. However, the assignments based on our double-resonance experiments are different from their results. It is necessary to reconsider the level structure for CH_3 torsion in the 9MA molecule.

The barrier height to CH_3 rotation in the S_0 state $V_6(S_0)$ in 9MA is remarkably larger than that in toluene. To elucidate the origin of torsional barrier, we carried out ab initio theoretical calculations at the higher level. The results were appreciably dependent on basis sets and calculational methods. We obtained the best results by the 6-31G** basis set and MP2 method, which yielded $V_6^{MP2}(S_0) = 162.6$ cm^{-1}. The stable conformation is staggered, and the barrier height is sufficiently close to the experimental value, 118 cm^{-1}. The calculated coordinates and Mulliken atomic charge of individual atoms are listed in Table 3 for both the staggered and eclipsed conformations. It can be seen that the geometrical structure of the anthracene frame is appreciably changed with the CH_3 rotation angle. The out-of-plane distortion is remarkable, particularly in the staggered conformation. It is considered to be due to coupling between the CH_3 torsion and out-of-plane normal vibrations in the anthracene moiety. It is noteworthy that the π molecular orbitals are also appreciably changed with the CH_3 rotational angle. The C_1-H_{16} and C_8-H_{24} bond lengths are not changed much, indicating that steric hindrance is not important. However, the C−C bond lengths in the anthracene π system are considerably different between the two conformations. This indicates that a potential barrier arises from the interaction between the π orbitals and the CH_3 group, that is, hyperconjugation. The decrease in V_6 upon electronic excitation is explained by the π orbitals illustrated in Figure 8. Although the π orbitals extend to the CH_3 moiety in both HOMO and LUMO, the coefficient in LUMO is smaller than that in HOMO. Consequently, the effect of hyperconjugation becomes small in the S_1 state, and the barrier height to CH_3 rotation is smaller than that of the S_0 state. Accurate theoretical calculations for the open shell at the high levels are desired to investigate the potential curve in the S_1 state quantitatively.

Methyl substitution often enhances the excited-state dynamics such as intramolecular vibrational redistribution (IVR). Broad emission could be found in the spectra for excitations of the 386 cm^{-1} band of 9MA-h_{12} and the 372 cm^{-1} band of 9MA-d_{12}. This indicates that IVR efficiently occurs, even in the levels of vibrational energies less than 400 cm^{-1}. This threshold excess energy is much lower than that of anthracene (1800 cm^{-1}).[24] It is very similar to the case of fluorotoluene.[4] The IVR in *p*-difluorobenzene starts at 1500 cm^{-1}, whereas it starts at 400

cm^{-1} in *p*-fluorotoluene. 9MA is also one of the typical examples to show the effect of methyl substitution on the enhancement of IVR. IVR is caused by mixing among the vibrational levels in an electronic state. The methyl substitution increases the number of low-frequency vibrational levels and lowers the molecular symmetry. Consequently, the density of coupling levels is remarkably increased, and the threshold excess energy becomes lower than that of the molecule without a methyl group.

In conclusion, we have observed the fluorescence excitation spectra and dispersed fluorescence spectra of 9MA-h_{12} and 9MA-d_{12} and confirmed the vibronic assignments by observing the double-resonance hole-burning spectrum of 9MA-h_{12}. We determined the energies of methyl torsional levels, which were fitted by a 1D potential curve with six-folded barriers. We obtained $V_6(S_0) = 118$ cm^{-1} and $V_6(S_1) = 33$ cm^{-1} for 9MA-h_{12}. These values of barrier height to methyl rotation are explained by hyperconjugation and coupling with an out-of-plane vibration. It has been show that IVR occurs in the vibrational level with the excess energy of 400 cm^{-1}. The enhancement by methyl substitution is attributed to an increase in level density.

Acknowledgment. This work was supported by Grant-in-Aid of Ministry of Education, Culture, Sports, Science, and Technology of Japan. We thank Mr. Hisashi Yoshida (Institute for Molecular Science) for his help in setting up the measurement system. We are grateful to Dr. Jon T. Hougen (NIST, Gaithersburg) for his helpful discussion and encouragement.

References and Notes

(1) Breen, P. J.; Warren, J. A.; Bernstein, E. R.; Seeman, J. I. *J. Chem. Phys.* **1987**, *87*, 1917–1926.
(2) Ishikawa, H.; Kajimoto, O.; Kato, S. *J. Chem. Phys.* **1993**, *99*, 800–809.
(3) Borst, D. R.; Pratt, D. W. *J. Chem. Phys.* **2000**, *113*, 3658–3669.
(4) Parmenter, C. S.; Stone, B. M. *J. Chem. Phys.* **1986**, *84*, 4710–4711.
(5) Moss, D. B.; Parmenter, C. S. *J. Chem. Phys.* **1993**, *98*, 6897–6905.
(6) Kiritani, M.; Yoshii, T.; Hirota, N.; Baba, M. *J. Phys. Chem.* **1994**, *98*, 11265–11268.
(7) Tan, X.-Q.; Majewski, W. A.; Plusquellic, D. F.; Pratt, D. W. *J. Chem. Phys.* **1991**, *94*, 7721–7733.
(8) de Haag, P. U.; Spooren, R.; Ebben, M.; Meerts, L.; Hougen, J. T. *Mol. Phys.* **1990**, *69*, 265–280.
(9) Nakagaki, M.; Nishi, E.; Sakota, K.; Nishi, K.; Nakano, H.; Sekiya, H. *Chem. Phys.* **2005**, *316*, 178–184.
(10) Mulliken, R. S. *J. Chem. Phys.* **1939**, *7*, 339–352.
(11) Hoffman, R. A. *Mol. Phys.* **1958**, *1*, 326–330.
(12) Baba, M.; Hanazaki, I.; Nagashima, U. *J. Chem. Phys.* **1985**, *82*, 3938–3947.
(13) Baba, M.; Nagashima, U.; Hanazaki, I. *J. Chem. Phys.* **1985**, *83*, 3514–3519.
(14) Syage, J. A.; Felker, P. M.; Semmes, D. H.; Al Adel, F.; Zewail, A. H. *J. Chem. Phys.* **1985**, *82*, 2896–2908.
(15) Tanaka, F.; Hirayama, S.; Yamashita, S.; Shobatake, K. *Bull. Chem. Soc. Jpn.* **1986**, *59*, 2011–2012.
(16) Stepanenko, Y.; Sobolewski, A. L.; Mordziński, A. *J. Mol. Spectrosc.* **2005**, *233*, 15–22.
(17) Nakagaki, M.; Nishi, E.; Sakota, K.; Nakano, H.; Sekiya, H. *Chem. Phys.* **2006**, *328*, 190–196.
(18) Longuet-Higgins, H. C. *Mol. Phys.* **1963**, *6*, 445–460.
(19) Bunker, P. R.; Jensen, P. *Molecular Symmetry and Spectroscopy*, 2nd ed.; NRC Research: Ottawa, Ontario, 1998.
(20) Hougen, J. T. *J. Phys. Chem.* **1986**, *90*, 562–568.
(21) Ishimoto, T.; Ishihara, Y.; Teramae, H.; Baba, M.; Nagashima, U. *J. Chem. Phys.* **2008**, *128*, 184309.
(22) Frisch, M. J. ; Trucks, G. A.; Schlegel, H. B.; Scuseria, G. E.; Robb, M. A.; Cheseman, J. R.; Montgomery Jr., J. A.; Vreeven, T.; Kudin, K. N.; Burant, J. C.; Millam, J. M.; Iyengar, S. S.; Tomasi, J.; Barone, V.; Mennuci, B.; Cossi, M.; Scalmani, G.; Rega, N.; Petersson, G. A.; Nakatsuji, H.; Hada, M.; Ehara, M.; Toyota, K.; Fukuda, R.; Hasegawa, J.; Ishida, M.; Nakajima, T.; Honda, Y.; Kitao, O.; Nakai, H.; Klene, M.; Li, X.; Knox, J. E.; Hratchian, H. P.; Cross, J. B.; Adamo, C.; Jaramillo, J.; Gomperts, R.; Stratmann, R. E.; Yazyev, O.; Austin, A. J.; Cammi, R.; Pomelli, C.; Ochtersky, J. W.; Ayala, P. Y.; Morokuma, K.; Voth, G. A.; Salvador, P.; Dannenberg, J. J.; Zakrzewski, V. G.; Dapprich, S.; Daniels, A. D.; Strain, M. C.; Farkas, O.; Malick, D. K.; Rabuck, A. D.; Raghavachari, K.; Foresman, J. B.; Ortiz, J. V.; Cui, Q.; Baboul, A. G.; Clifford, S.; Cioslowski, J.; Stefanov, B. B.; Liu, G.; Liashenko, A.; Piskorz, P.; Komaromi, L.; Martin, R. L.; Fox, D, J.; Keith, T.; Al-Laham, M. A.; Peng, C. Y.; Nanayakkara, A.; Challacombe, M.; Gill, P. M. W.; Johnson, B.; Chen, W.; Wong, M. W.; Gonzalez, C.; Pople, J. A. *Gaussian 03*, revision B.05; Gaussion, Inc., Pittsburgh PA, 2003.
(23) Herzberg, G. *Electronic Spectra and Electronic Structure of Polyatomic Molecules*; Molecular Spectra and Molecular Structure, Vol. III; Van Nostrand Reinhold: New York, 1966.
(24) Lambert, W. R.; Felker, P. M.; Zewail, A. H. *J. Chem. Phys.* **1984**, *81*, 2209–2216.

JP808550R